Journal of Power Sources 201 (2012) 332–339

Contents lists available at SciVerse ScienceDirect

Journal of Power Sources

journal homepage: www.elsevier.com/locate/jpowsour

# Novel $Pr_{0.6}Sr_{0.4}Fe_{0.8}Co_{0.2}O_3$:$Ce_{0.8}Sm_{0.2}O_2$ composite nanotubes for energy conversion and storage

Ricardo Pinedo[a], Idoia Ruiz de Larramendi[a], Nagore Ortiz-Vitoriano[a], Izaskun Gil de Muro[a], Teofilo Rojo[a,b,*]

[a] Departamento de Química Inorgánica, Facultad de Ciencia y Tecnología, Universidad del País Vasco UPV/EHU, Apdo. 644, 48080 Bilbao, Spain
[b] CIC energiGUNE, Parque Tecnológico, Albert Einstein, 48, 01510 Miñano, Álava, Spain

ARTICLE INFO

*Article history:*
Received 17 August 2011
Received in revised form 20 October 2011
Accepted 24 October 2011
Available online 3 November 2011

*Keywords:*
Solid oxide fuel cell
Nanomaterial
Perovskite
Fluorite
Electrochemical impedance spectroscopy

ABSTRACT

One of the most important challenges for further development of solid oxide fuel cells is to design new electrodes which operate at intermediate temperatures. In this sense, the formation of nanostructures of the $Pr_{0.6}Sr_{0.4}Fe_{0.8}Co_{0.2}O_3$:$Ce_{0.8}Sm_{0.2}O_2$ composite and their characterization have been carried out. These nanostructures have been synthesized using polymeric membranes with 0.1 μm pore size as templates. The electronic microscopy has been used in order to confirm the dimensions of the obtained nanotubes with a wall thickness of 20 nm. The impedance spectroscopy measurements reveal the good performance of these nanostructured materials and the effect that the nanostructures and the addition of a pure ionic conductor have on the electrochemical performance. The synthesized nanostructured composite exhibits an area specific resistance (ASR) value smaller than that obtained for the sample without the nanostructured morphology together with the addition of the pure ionic conductor.



## 1. Introduction

The scientific research is focusing their interest on the development of energy related devices looking for possible alternatives to solve the energetic dependence of petrol. Some of the most promising devices are lithium batteries and fuel cells [1]. In addition, the supercapacitors are other energy storage alternative. Nanostructured materials emerge as potential materials to enhance the performance of these systems [2–4].

The field of fuel cells has been researched for decades because they enable the direct conversion of chemical energy into the electrical one. The proton exchange membrane fuel cells (PEMFC) and the solid oxide fuel cells (SOFC) are the fuel cell types which exhibit the more interesting characteristics for technological devices. The main advantages that the SOFCs present are their high efficiencies and the fuel flexibility [5]. However, lower operating temperatures are necessary in order to be a realistic and commercially energetic alternative [4]. This temperature decrease allows the reduction of the manufacturing costs and the increase of the cell durability [5–8].

In order to be used as SOFC electrodes, the materials must fulfil the following requirements: good electronic and ionic conductivity, adequate porosity, thermal and chemical compatibility with the electrolyte, and stability with time [9]. Although there are many materials which satisfy these conditions for their application as SOFC electrodes, the perovskite-type oxides are the most promising, and therefore studied, materials [10–13]. Nevertheless, both the mentioned conditions of the SOFC electrodes and the reduction of the temperature can be also taken into account. For that purpose, two leading approaches are being widely researched: the optimization of the microstructure and the synthesis of composite materials. In the field of the microstructural optimization, the nanomaterials are being employed due to its great active area [14,15]. In addition, the influence that the different morphologies in the nanometric scale could have on the electrochemical performance of these cells is also considered and studied [16,17]. On the other hand, the composite materials are also of a great interest due to the improvement of the ionic conductivity that can achieve when the perovskite oxide is mixed with a pure ionic conductor [18,19]. Furthermore, this mixture could also provide an improvement in the thermal stress of the fuel cell stack, if the thermal expansion coefficients of the electrolyte and the composite cathode are closer to each other than without considering the addition of the pure ionic conductor [20–22].

The aim of this work is to join these two approaches (the microstructural optimization and the synthesis of composite materials) in order to obtain a new material with potential application in the intermediate temperature solid oxide fuel cells (IT-SOFCs) which operate in the range of 500–700 °C. For this purpose, the

* Corresponding author at: Departamento de Química Inorgánica, Facultad de Ciencia y Tecnología, Universidad del País Vasco UPV/EHU, Apdo. 644, 48080 Bilbao, Spain. Tel.: +34 94 6012458; fax: +34 94 6013500.
*E-mail address:* teo.rojo@ehu.es (T. Rojo).

0378-7753/$ – see front matter © 2011 Elsevier B.V. All rights reserved.
doi:10.1016/j.jpowsour.2011.10.089

$Pr_{0.6}Sr_{0.4}Fe_{0.8}Co_{0.2}O_3$ (PSFC)–$Sm_{0.2}Ce_{0.8}O_2$ (SDC) composite nanotubes were synthesized using soft templates of polycarbonate with micropores. The powerful non difficult and economical route to synthesize nanostructured materials presented herein enables the attainment of materials with great surface area, and consequently, good electrochemical behaviour. This way, this synthetic route gives rise to the attainment of materials with excellent properties for their application in both energy conversion systems as solid oxide fuel cells and energy storage devices as lithium batteries and supercapacitors.

## 2. Experimental

### 2.1. Synthesis of $Pr_{0.6}Sr_{0.4}Fe_{0.8}Co_{0.2}O_3$/$Sm_{0.2}Ce_{0.8}O_2$ nanotubes

The $Pr_{0.6}Sr_{0.4}Fe_{0.8}Co_{0.2}O_3$ (PSFC) perovskite-type oxide precursor and the samarium doped ceria (SDC) have been synthesized by the conventional sol–gel route. This technique has been particularly investigated because it provides the attainment of very fine powders with a low agglomerating degree together with its simplicity to apply this technique in the use of membrane templates [23,24]. Commercial polycarbonate membranes (Millipore) with porous diameter of 0.1 μm have been used as template in order to synthesize nanotubes with nanometer scale dimensions [25]. Metal nitrate salts were used as the starting materials for the final product and citric acid as chelating agent. $Pr(NO_3)_3.5H_2O$, $Sr(NO_3)_2$, $Fe(NO_3)_3{\cdot}9H_2O$ and $Co(NO_3)_2{\cdot}6H_2O$ (Sigma–Aldrich) were weighed stoichiometrically according to the nominal composition of $Pr_{0.6}Sr_{0.4}Fe_{0.8}Co_{0.2}O_3$, while $Sm_2O_3$ and $Ce_3(NO_3)_3{\cdot}6H_2O$ were employed for the synthesis of the SDC. Then, these nitrates were dissolved in distilled water adding later the citric acid and ethylene glycol into the solution. Once the solutions were completely dissolved they were mixed together and homogenised. Subsequently the solution was poured onto the polycarbonate membranes. A heating process at 700 °C in air was carried out in order to remove the polymeric templates and reach the crystallization of the compounds. Bellino et al. reported that a thermal treatment slightly above the crystallization temperature could improve the mechanical resistance of the nanotubes without affecting the sinterization (or surface area) of the nanostructures [26].

### 2.2. Structural characterization

The X-ray powder diffraction (XRD) data were used to characterize the obtained crystal structure of the as-calcined materials, using a Philips PW1710 diffractometer, with $CuK_\alpha$ radiation and a scanning step 0.02° (2$\theta$) over the angular range 5–70° (2$\theta$). The obtained data were fitted using the FULLPROF program [27].

The pairing of oxide ion conducting electrolytes with chemically compatible electrode materials is very important to the performance of SOFCs. In this way, chemical compatibility tests were performed to determinate the interaction between the cathode and the electrolyte. For this purpose, PSFC and SDC powders were intimately mixed (weight ratio of 1:1) and isopressed to form a pellet. These pellets were fired at different temperatures for one week. Quartz was used as standard material. Then, it was characterized by XRD to investigate the appearance of any reaction products.

Thermal expansion measurements as a function of temperature up to 1000 °C in air were carried out with a LINSEIS vertical dilatometer (L75 Platinum Series). The phases were prepared as dense sintered compounds exhibiting coplanar surfaces.

### 2.3. Microstructure analysis

The powder morphology was examined by transmission electron microscopy (TEM) using a Philips CM200 transmission electron microscope and by field emission scanning electron microscopy (FESEM) with Schottky emitter using a JEOL JSM-7000F microscope at 20 kV accelerating voltage.

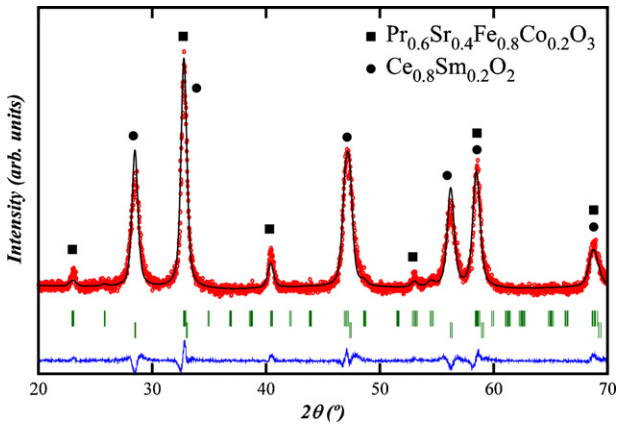


**Fig. 1.** Fitted diffraction profile of PSFC:SDC showing observed (crosses), calculated (line) and difference (lower) profiles.

### 2.4. Electrochemical measurements

The electrical conductivity of sintered bars of approximate 1 mm × 3 mm × 7 mm dimensions was measured in air from 500 to 800 °C at 50 °C intervals by the Van der Pauw's four probe technique. Electrical contacts were made using Pt wires and Pt paste placed over whole end faces ensuring a homogeneous current flow. The conductivity ($\sigma$) was determined from a set of $V$–$I$ values by taking $\sigma = 1/\rho = L/A \times dI/dV$, where $L$ is the distance between voltage contacts and $A$ is the sample cross section. A current load of 5–100 mA was applied with a Keithley 6221 DC and AC current source. The corresponding voltage drop was recorded with a 2182A nanovoltimeter.

Electrochemical characterization of the nanostructured composite cathode was carried out by means of impedance spectroscopy using a two-electrode configuration, being necessary to obtain the impedance spectra for symmetrical cells. In this manner, the cells were performed of electrolyte pellets onto which symmetrical electrodes were deposited. Synthesized electrolyte (Sm-doped ceria, SDC) and platinum as current collector have been used. The SDC powder was pressed under 10 T uniaxial forces to form green pellets. The pellets were sintered at 1050 °C (4 h) and subsequently at 1500 °C (4 h). The density of the obtained pellets is higher than 93% opposite to the theoretical value. The surface of the pellets was polished with grit paper and then cleaned with ethanol and acetone solutions. In order to prepare the electrodes, the obtained nanostructured composites were dispersed in a vehicle ink in a 1:1 weight ratio forming a paste. This paste was painted with a paintbrush in both faces of the pellets forming symmetrical cells which were sintered at 1000 °C for 4 h to form porous electrodes well adhered to the surface of the electrolytes.

Electrochemical impedance spectroscopy (EIS) measurements of symmetrical test cells were conducted using a Solartron 1260 Impedance Analyzer. The frequency range was $10^{-2}$–$10^6$ Hz with an AC perturbation signal of 50 mV. All these electrochemical experiments were performed at equilibrium from room temperature up to 700 °C and down to room temperature, under both zero dc current intensity and air.

## 3. Results and discussion

The obtained diffractogram reveals the presence of two different phases in each nanotube (Fig. 1). The orthorhombic phase

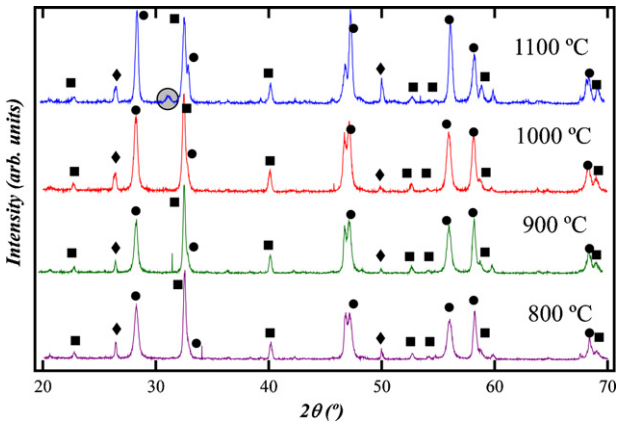


**Fig. 2.** X-ray diffraction patterns of equimolecular PSFC/SDC mixtures after annealing in air at different temperatures for 1 week (■, PSFC; ●, SDC; ♦, quartz).

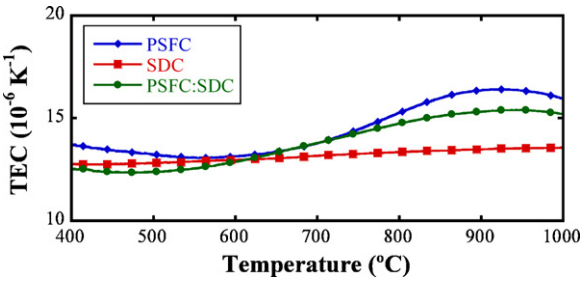


**Fig. 3.** Thermal expansion coefficients (TEC) measured in air for PSFC, SDC and PSFC:SDC samples in the temperature range between 400 and 1000 °C.

corresponds to the perovskite-type oxide PSFC (space group *Pbnm*), which is similar to $GdFeO_3$, while the cubic phase corresponds to the SDC (space group *Fm-3m*). The obtained cell parameters for the perovskite type structure are $a = 5.4733$ Å, $b = 5.4716$ Å, $c = 7.7385$ Å. In turn, the cell parameters achieved for the SDC are $a = b = c = 5.4178$ Å. Percentages of perovskite and fluorite phases can be obtained from the fitting of X-ray diffraction data, taking into account the total integrated intensity. This way, the ratio of PSFC to SDC in the composite nanotubes is 12% of the fluorite phase and 88% of the PSFC phase, which agrees with the theoretical composition.

The reactivity of perovskite materials with most electrolytes, which leads to the formation of secondary phases, can affect the electrical conductivity along either the nanostructured composite or the cathode/electrolyte interface. This is an important problem that must be taken into consideration in the use of these materials for SOFC applications [9,28,29]. Due to chemical reactions between the perovskite and the ionic conductor, secondary phases usually appear at elevated temperatures during the processing and fixation of the cell components. PSFC sample and SDC electrolyte were mixed together to form a pellet which was sintered at 800, 900, 1000 and 1100 °C during a week to study their chemical compatibility. XRD patterns of the chemical reactivity test are shown in Fig. 2. After calcination at temperatures up to 1000 °C, no extra diffraction peaks appear indicating that no significant chemical reactions occur between both materials. In contrast, at 1100 °C, diffraction reflexions corresponding to secondary phases are detected (see the new peak observed at 31°). In this way, we can ensure the presence of a high moisture tolerance of PSFC:SDC composite cathodes at temperatures below 1000 °C.

Another important factor to be considered is the thermal expansion coefficient (TEC). The TEC values for cathodic materials must be similar to that of the electrolyte in order to avoid the thermal stresses which can cause delamination and cracks, leading to a poorer adhesion of the components. The TEC value of the PSFC:SDC composite was determined by dilatometry and compared with the thermomechanical properties of the PSFC and SDC materials (Fig. 3). It is worth mentioning that these experiments have been carried out in dense bars. This fact implies the destruction of the obtained nanotube shaped structure, as a consequence of the sinterization process. Nevertheless, the TEC data of the material allow knowing whether the selected cathodic material, in bulk, and the electrolyte are compatible for SOFC applications. So, these data can be extrapolated as estimation to the nanostructured material. The SDC electrolyte exhibits very stable thermomechanical behaviour along the measured temperature range. In contrast, the TEC value of PSFC strongly depends on temperature, showing a decrease between 400 and 600 °C. This anomalous behaviour can be attributed either to the presence of a phase transition where the cell volume decreases or changes in the oxidation states of Pr and Fe. In order to determine the presence of a possible phase transition, diffraction patterns at different temperatures were recorded. The results indicated that the perovskite phase was stable during the experiment, being possible to ensure that no structural changes were produced. In this manner, a change in the oxidation states of Pr and/or Fe accompanied by a loss of oxygen is expected, giving rise to an expansion of the crystal lattice. This fact is in good agreement with the results previously reported by Yin et al. [30]. The curvature change in the composite is smoother than that observed in the PSFC sample, showing an atypical behaviour also observed in the PSFC:SDC composite. When SDC is added to the PSFC powder (1:1 weight ratio), the TEC value decreases from $14.83 \times 10^{-6}\,K^{-1}$ to $13.74 \times 10^{-6}\,K^{-1}$, indicating that PSFC becomes more compatible with the SDC electrolyte for the composite phase, as reported by other authors [31–33].

The morphology of the synthesized samples is given in Fig. 4. The images show nanostructured morphology homogenously distributed along the sample (Fig. 4c). Looking at the images with more detail, the diameters and length of the perovskite nanotubes can be observed (Fig. 4a). The PSFC: SDC hollow 1D nanotubes present nanoscale dimensions with diameters between 45 and 60 nm. These nanotubes are single walled measuring a few nanometers in diameter (controlled by the dimension of the template) and several microns in length.

The TEM images reveal the presence of nanotubes with the thickness and length limited by the template dimensions (Fig. 5). The external surface of these nanotubes is rough, and the different nanoparticles which form the nanotubes can be easily detected. The observed roughness could promote the increase of the surface area caused by the nanostructured morphology. The existence of small pores along the wall of the nanotube will produce a higher contact between oxygen and the cathodic material, giving rise to a larger amount of double phase boundaries (gas/cathode interface) which enhance the electrochemical performance of the system [34,35]. The crystallite size of the nanoparticles is below 20 nm fitting well with the wall thickness of the nanotubes (Fig. 5c and d), in good agreement with previous results obtained in our laboratory [17]. Energy-dispersive X-ray spectroscopy (EDX) was used to visualize the element profiles in the nanotubes. EDX analysis demonstrated that stoichiometry was formed for both phases in each nanotube. In order to identify the grains corresponding to each phase in the nanotubes, electron diffraction patterns were recorded. The high degree of sinterization suffered by the grains and the similarity between d spaces of both phases, make not possible the identification of each phase.

The electrochemical tests of this nanostructured composite material have been carried out at high temperatures. The nanotubes could suffer a collapse after high temperature sintering (at 1000 °C). The morphology of the cathodic material after electrochemical tests is shown in Fig. 6. A good adhesion of the cathode on

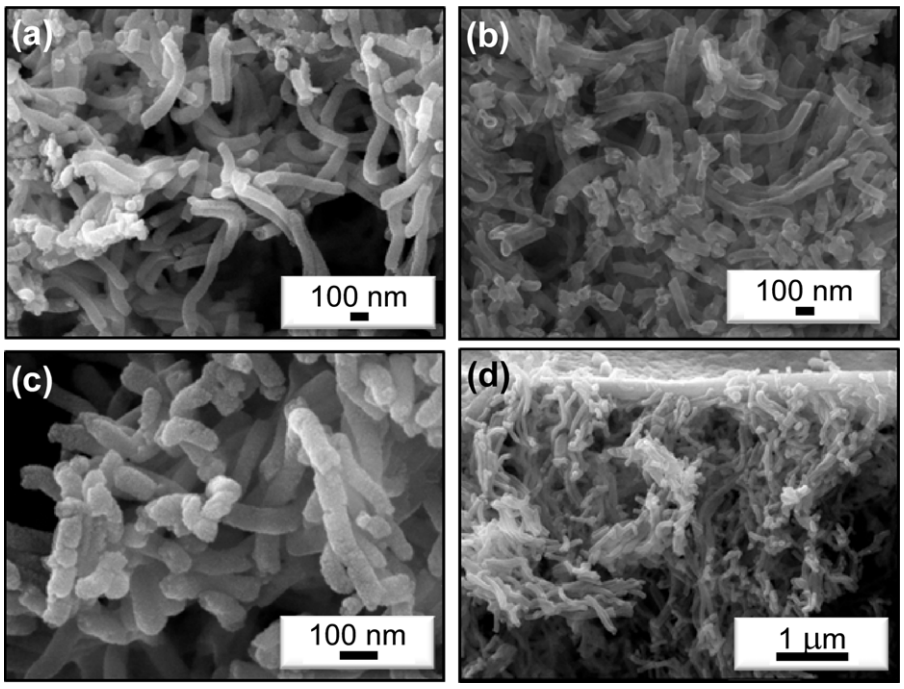


**Fig. 4.** SEM images of the morphology of the PSFC:SDC nanotubes.

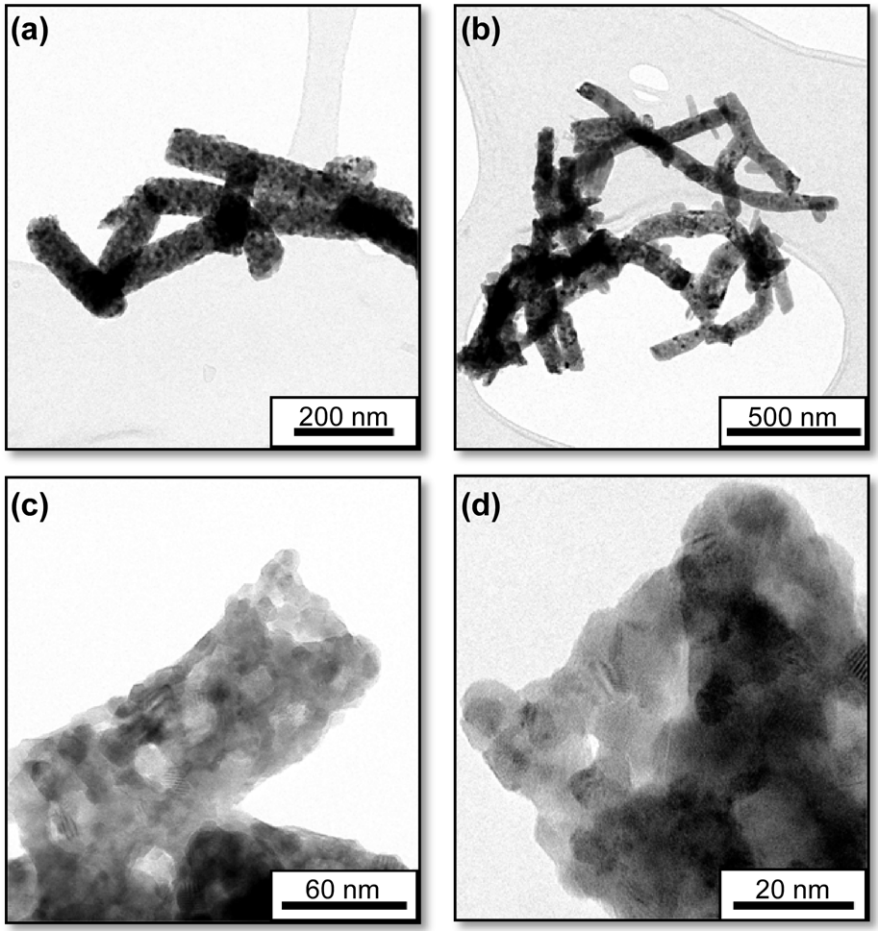


**Fig. 5.** TEM images of the morphology of the PSFC:SDC nanotubes.

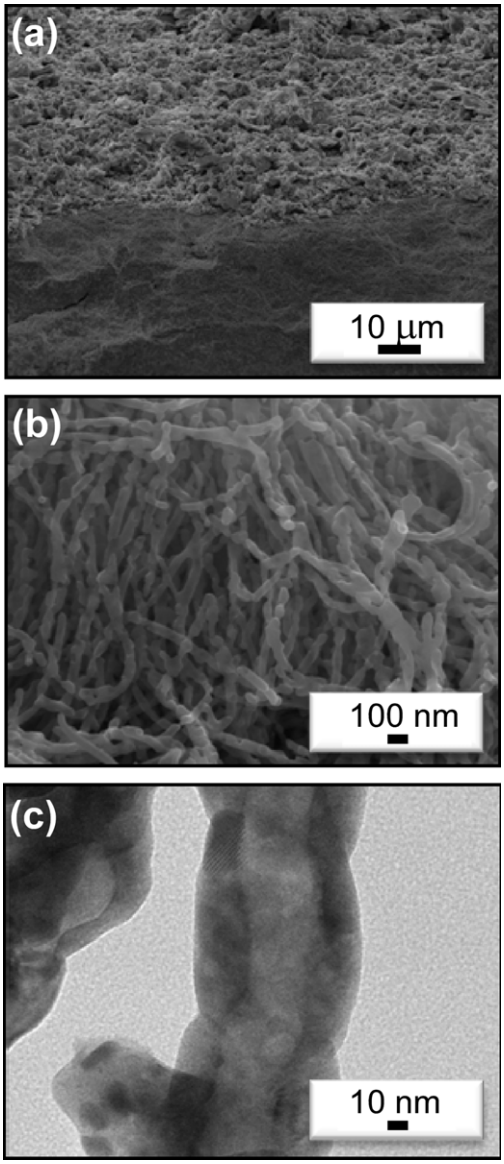


**Fig. 6.** (a and b) SEM and (c) TEM images of the morphology of the PSFC:SDC nanostructured material after electrochemical tests.

the surface of the electrolyte is observed, giving rise to the existence of an optimum cathode/electrolyte interface. As shown in Fig. 6b, the nanostructure of the material is maintained and the nanotubes do not experiment any collapse after sintering temperature. As can be expected, the porosity of the walls of the nanotubes has been reduced. After the electrochemical tests, the obtained nanotubes have denser walls due to the growth of the grains, but maintaining the nanotube shape (see Fig. 6c).

The electrical conductivities for the PSFC and PSFC:SDC samples performed in air are shown in Fig. 7. For these experiments, dense pellets were obtained in order to get data directly referred to the bulk material and not to the nanostructured synthesized samples. Conductivity measurements were carried out in order to deduce the potential application of the materials as cathodes being the required conductivity $\sigma$ higher than 100 S cm$^{-1}$. In addition, if the bulk material fulfils this requirement, it is supposed that the nanostructured material also satisfies this condition. The electrical conductivity of PSFC first increases, reaching a maximum at 600 °C and after that it decreases with increasing temperature. At temperatures lower than 600 °C, where the electrical conductivity

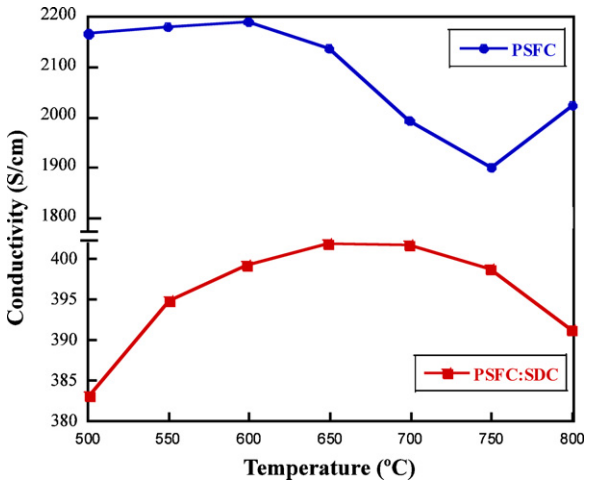


**Fig. 7.** Variation of the electrical conductivity with temperature for the PSFC and PSFC:SDC materials.

maximum is observed, a small-polaron semiconducting behaviour is found. The decrease in conductivity after 600 °C could be assigned to the loss of oxygen from the lattice at high temperatures. This result agrees with the behaviour described in the dilatometric measurements and those observed in the literature for other related compounds [36,37]. At low temperatures, the conduction is meanly electronic and is produced by the charge compensation, where some Fe cations change from trivalent to tetravalent oxidation state. At higher temperatures, ionic compensation becomes significant as the oxygen content of the material decreases. The PSFC sample exhibits a conductivity of 2190 S cm$^{-1}$ at 600 °C, one of the highest conductivities for similar compounds described in the literature [38]. Furthermore, on having mixed the PSFC sample with SDC, a drop in the electrical conductivity (400 S cm$^{-1}$ at 600 °C) is obtained. This fact can be explained by the introduction of an ionic conductor (SDC) in the PSFC sample. The PSFC:SDC composite exhibits an increasing conductivity with the temperature up to 650 °C. The electronic conductivity of the PSFC:SDC composite is over 100 S cm$^{-1}$ over a wide temperature range, satisfying the general requirement for electrode materials in intermediate temperature SOFC. Sm-doped ceria (SDC) is considered to be a promising electrolyte for low temperature SOFC. One of the drawbacks associated to this material is related to the partial reduction of $Ce^{4+}$ to $Ce^{3+}$ at intermediate temperature (>600 °C), which leads to electronic conductivity that reduces performance due to electronic leakage currents between the anode and cathode. In the PSFC:SDC composite, the partial reduction of cerium in the SDC material is an advantage because an increase in electronic conductivity is caused at temperatures above 600 °C, giving rise to a maximum conductivity for the PSFC:SDC composite of 402 S cm$^{-1}$ at 650 °C. The temperature dependence of the electronic conductivity is relatively strong, as quantitatively expressed by the activation energy of about 0.085 eV for the title compound. The conductivity of PSFC fits well according to a small polaron mechanism at lower temperatures ($E_a$ = 0.068 eV) but start deviating from linearity at approximately 650 °C increasing the $E_a$ value to 0.0998 eV. These results agree with those reported in the literature for Co containing perovskites [39].

The impedance spectra for PSFC:SDC/SDC/PSFC:SDC cell measured in air at different temperatures during the heating (H) and cooling (C) processes are shown in Fig. 8a. In the Nyquist plots, the existence of two depressed semicircles indicates that at least two different processes related to the oxygen reduction reaction (ORR) might take place. Investigation of the ORR mechanism is important for the improvement of the electrochemical

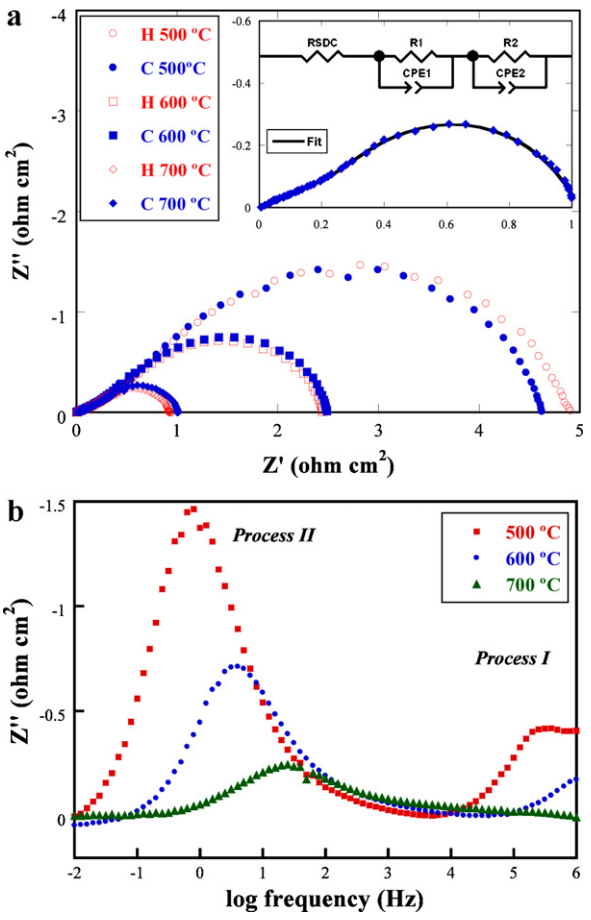


**Fig. 8.** (a) Nyquist diagram of the PSFC:SDC nanostructured composite at different temperatures (H, heating process; C, cooling process). The impedance data are plotted after electrolyte ohmic drop correction for comparison of polarization resistance. (b) Bode plot of the variation of the imaginary part of impedance as a function of frequency at different temperatures.

properties of SOFCs. Fig. 8b shows the log-frequency dependence of the impedance part ($Z''$) of PSCF:SDC electrode on SDC electrolyte measured at different temperatures. The curves show two maxima at high ($10^5$ Hz) and low (1–$10^2$ Hz) frequencies. The contribution at high frequencies (Process I) corresponds to a process related to the electrode/electrolyte interface and not to the electrode surface. However, the low frequency arc (Process II) is ascribed to the dissociative adsorption of $O_2$ followed by electrochemical reduction and transfer of oxygen species at the triple phase boundary (TPB) [40]. As can be observed in Fig. 8b, the symmetric cell is dominated by the low frequency arc. This process shifts to higher frequencies with increasing temperature from 1 to $10^2$ Hz. indicating the existence of a thermally activated process [41].

In order to elucidate the conducting processes occurring in the composite/electrolyte system, impedance data have been fitted using the equivalent circuit shown as inset in Fig. 8a. The equivalent circuit represents three different contributions which result in the total resistance of the system. R-SDC corresponds to the ohmic resistance of the electrolyte, R1 is due to charge transfer and R2 is attributed to dissociative adsorption on the electrode surface and gas diffusion [25,42]. R1 and R2 have constant phase elements (CPE) in parallel to simulate the distribution of relaxation time in the real system.

The high-frequency arc (R1) is assigned to the charge transfer of oxide species across the electrode/electrolyte interface [43–45]. The semicircle of medium-low frequencies (R2) is attributed to the surface diffusion ($O_{ad}{}^{-} \rightarrow O_{electrode/electrolyte}{}^{-}$) [46,47]. The oxide

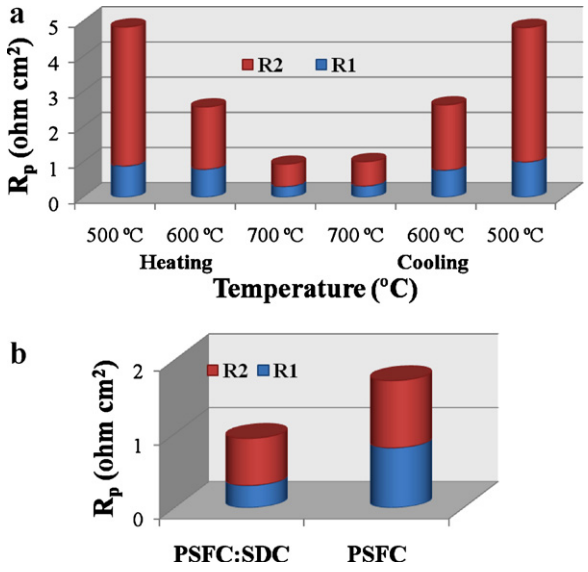


**Fig. 9.** Comparative evolution of the polarization resistances (a) during the cycle of heating and cooling down the cell and (b) between PSFC:SDC nanostructured composite and PSFC nanotubes at 700 °C ($R_p$: polarization resistance).

ions formed in the double and triple phase boundary (DPB and TPB) sites must move to the interface electrode/electrolyte to be able to cross the electrolyte. The contribution due to the gas diffusion process that can be observed usually at low frequencies is overlapped with the surface diffusion process making difficult to distinguish it. Anyway, using the equivalent circuit proposed in this work, it is possible to assign a resistance to each process (R1 and R2), as shown in Fig. 9a. By comparing the evolution of the resistances with the temperature, two conclusions can be deduced: (i) there are no changes in the resistance values when the heating and cooling cycles are analysed and (ii) the major contribution to the polarization resistance (R1 + R2) is caused by the R2 process. This way, the dominant resistive process (R2) is the electrochemical resistance associated with the oxygen exchange at the surface of the cathodic electrode. The corresponding semicircle in the impedance spectra is observed at low frequencies (right side of the Nyquist plot), indicating a large capacitance. As stated before, R2 is associated to diffusion processes (adsorption–desorption of oxygen, oxygen diffusion at the gas/cathode surface interface and surface diffusion of intermediate oxygen species) [48]. All these processes are related to the surface, while the R1 contribution is assigned to the conduction across the bulk material. At low temperatures (500 °C) the contribution due to diffusion processes (R2) is dominant and limiting process. Oxygen atom must be dissociated into oxide ion before diffusion, needing this reaction a thermal energy to overcome the activation barrier. The energy absorbed at low temperatures is not enough to compensate this barrier, giving rise to a slower kinetic.

If the R1 and R2 resistances of the nanostructured PSFC:SDC composite are compared with those of the PSFC nanotubes (see Fig. 9b), an important decrease of R1 value can be clearly distinguished [17]. Consequently, when nanocomposite is tested an improvement in conduction across the bulk is obtained while contribution related to the surface (R2) is almost the same. Although the PSFC is a MIEC material, the addition of an ionic conductor as the SDC improves the transport of the formed oxide ions through the material, as shown in Fig. 10. This fact implies that the charge transfer processes at the interfaces (current collector/cathode and cathode/electrolyte interfaces), can easily occur in the nanostructured composite across the wall of the nanotube. This resistance may be related to reaction kinetics determined by the electrochemical activity of the cathodic material, electrical

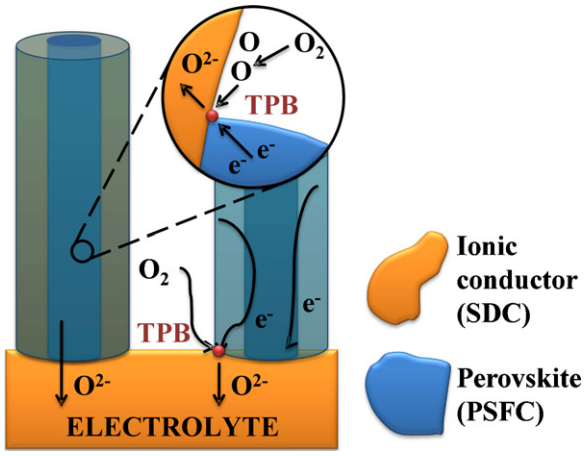


**Fig. 10.** Schematic diagram of the different processes that take place in PSFC:SDC nanocomposite and PSFC nanotubes (MIEC, mixed ionic and electronic conductor; TPB, triple phase boundary).

conductivity of electrode/current collector, and ionic conductivity of electrode/electrolyte [30]. Taking these considerations into account, the decrease observed in R1 indicates a good interconnectivity between PSFC and SDC grains along the nanotube in the PSFC:SDC composite.

In order to normalize the obtained polarization resistance values, the area specific resistance value (ASR) has been calculated taking into account the measured area, as shown in Fig. 11. The polarization resistance decreases dramatically with increasing temperature obtaining ASR values as good as 0.46 $\Omega\,cm^2$ at 700 °C for the PSFC:SDC nanotube structured composite. It is worth mentioning, that at 700 °C, the nanostructure is maintained and the growth of the crystallites could be negligible [17]. The ASR values obtained in the present study are comparable even better than those reported in the literature [32,49,50]. The good behaviour exhibited by the PSFC:SDC nanocomposite indicates that this cathode can be used for the intermediate temperature SOFCs.

In a previous work, PSFC nanoparticles were obtained using carbon nanotubes as grain size controllers [51]. The obtained PSFC nanoparticles exhibit lower polarization resistance than that of the PSFC:SDC nanotubes presented in this work. This fact is due to the existence of SDC particles in the surface of the composite nanotubes. These particles are mainly ionic conductors, which implies that the oxygen reduction will not be carried out where the SDC nanoparticles are located, reducing therefore the performance of the cathodic material. However, these nanotubes are supposed to be more structurally stable than the mentioned nanoparticles under the operation temperatures of the cell. It is worth mentioning that the operation temperature will produce a sinterization of the nanoparticles with time, and therefore, their surface area will be decreased. In the case of the nanotubes, the effect of the sinterization process is supposed to be not so strong. On the other hand, the addition of the SDC to the cathodic material implies an improvement in the compatibility between the cathode and the electrolyte which leads to mechanical advantages.

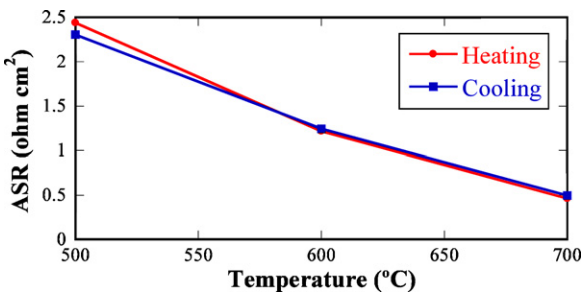


**Fig. 11.** Thermal evolution of the area specific resistance (ASR) during the heating and cooling processes.

Other similar materials have been proposed as SOFC cathodes. Park et al. studied the effect of the sintering temperature on the electrochemical response of $Pr_{0.3}Sr_{0.7}Co_{0.3}Fe_{0.7}O_{3-\delta}$ [31]. They obtained ASR values as good as 0.115 $\Omega\,cm^2$ at 700 °C when cathode is sintered at 1200 °C. In our case, taking into account the reactivity study, the higher sintering temperature that can be used is 1000 °C. Park et al. obtained an ASR value of about 2.5 $\Omega\,cm^2$ at 700 °C when cathodes were sintered at 1000 °C. The decrease in the cathodic performance when CGO ($Gd_{0.1}Ce_{0.9}O_2$) is added was also observed by these authors.

Several authors have tried to improve the performance of the cathodes by nanostructuring composite materials [52–54]. It is worth mentioning the interesting results obtained by Zhang et al. with similar composite nanotubes made of $La_{0.8}Sr_{0.2}MnO_{3-\delta}$ (LSM)/$Zr_{0.92}Y_{0.08}O_2$ (YSZ) [52]. Anyway, the drawback associated to this kind of composite nanotubes is to control the diffusion of oxide ions trough the ionic conductor. The grains of the fluorite phase must be interconnected and provide to the ions an easy way to the electrode/electrolyte interface. In order to solve this point, Zhi et al. proposed a new design consisting on YSZ nanofiber scaffold with the infiltrated LSM where the continuous nanofibers provide an uninterrupted path that facilitates the charge transport [54]. Using this novel design, a polarization resistance of 0.48 $\Omega\,cm^2$ at 700 °C is reported, similar to that obtained for PSFC:SDC composite nanotubes. Infiltrated nanofibers have also been used for improving the performance of SOFC anodes [55].

Most of SOFC cathodes based on Co such as $Ba_{0.5}Sr_{0.5}Co_{0.8}Fe_{0.2}O_3$ present larger surface area for the oxygen reduction reaction, not restricted to the vicinity of the three phase boundary (cathode/air/electrolyte) [56]. The drawback associated to this kind of Co containing oxides is the high thermal expansion coefficients (TEC) [57]. The composite described in this paper presents excellent performance as shown in the electrochemical impedance measurements. The greatly improved performance of this novel material is related to two main issues: (i) creation of composite cathodes looking for an enhancement of the ionic conduction through the cathodic material and (ii) integration of different composition nanoparticles in a nanostructure with a high surface-to-volume ratio, without using organic binders, increasing the active area of the material. Another additional advantage is the low thermal expansion coefficient obtained for these compounds, with TEC values of $13.74 \times 10^{-6}\,K^{-1}$, making these materials compatible with samarium doped ceria (SDC) electrolyte and Ni-SDC anodes.

## 4. Conclusions

The data presented herein show that the use of nanotubes of the PSFC:SDC composite as cathode for intermediate temperature solid oxide fuel cells can deliver an area specific resistance (ASR) value of 0.46 $\Omega\,cm^2$ at 700 °C. This value significantly improves the performance of conventional cathodes in these devices. By nanostructuring the electrode material, an increase of the active area is obtained, giving rise to a larger amount of double phase boundaries (DPB) where gas and cathode meet. Besides, by the addition of the pure ionic conductor (Sm-doped ceria, SDC), a creation of triple phase boundaries (TPBs) is obtained.

The new synthetic route described for this compound contributes to the scientific research opening a new perspective in the utilization of the nanotechnology, designing nanomaterials, in which several parameters as the pore size and distribution, surface

area or functionalization of the surface can be controlled. These parameters have a great influence on the performance of the materials used for energy conversion and storage, which means that this method is an important starting point for the design and optimization of these types of energy devices.

## Acknowledgements

This work has been partially financed by the Spanish CiCyT under project MAT2010-19442 and by the Government of the Basque Country under project IT-312-07 and SAIOTEK S-PE09UN61. R. Pinedo thanks the Universidad del País Vasco (UPV/EHU) for his predoctoral fellowship. N. Ortiz-Vitoriano thanks the Eusko Jaurlaritza/Gobierno Vasco for their predoctoral fellowship.

## References

[1] M. Armand, J.M. Tarascon, Nature 451 (2008) 652–657.
[2] (a) P.G. Bruce, B. Scrosati, J.M. Tarascon, Angew. Chem. Int. Ed. 47 (2008) 2930–2946;
(b) C. Liu, F. Li, L.P. Ma, H.M. Cheng, Adv. Mater. 22 (2010) E28–E62.
[3] (a) B.C.H. Steele, A. Heinzel, Nature 414 (2001) 345–352;
(b) N.P. Brandon, S. Skinner, B.C.H. Steele, Annu. Rev. Mater. Res. 33 (2003) 183–213.
[4] J.C. Ruiz-Morales, D. Marrero-López, M. Gálvez-Sánchez, J. Canales-Vázquez, C. Savaniu, S.N. Savvin, Energy Environ. Sci. 3 (2010) 1670–1681.
[5] B.C.H. Steele, Nature 400 (1999) 619–621.
[6] T. Hibino, A. Hashimoto, T. Inoue, J. Tokuno, S. Yoshida, M. Sano, Science 288 (2000) 2031–2033.
[7] S.D. Park, J.M. Vohs, R.J. Gorte, Nature 404 (2000) 265–267.
[8] Z.P. Shao, S.M. Haile, Nature 431 (2004) 170–173.
[9] G. Zhu, X. Fang, C. Xia, X. Liu, Ceram. Int. 31 (2005) 115–119.
[10] E.P. Murray, M.J. Sever, S.A. Barnett, Solid State Ionics 148 (2002) 27–34.
[11] A. Aguadero, J.A. Alonso, M.J. Escudero, L. Daza, Solid State Ionics 179 (2008) 393–400.
[12] C. Lalanne, G. Prosperi, J.M. Bassat, F. Mauvy, S. Fourcade, P. Stevens, M. Zahid, S. Diethelm, J. Van Herle, J.C. Grenier, J. Power Sources 185 (2008) 1218–1224.
[13] A. Tarancón, J.P. Martínez, D.M. López, A. Morata, J.C. Ruiz-Morales, P. Núñez, Solid State Ionics 179 (2008) 2372–2378.
[14] D. Marrero-López, J.C. Ruiz-Morales, J. Peña-Martínez, J. Canales-Vázquez, P. Núñez, J. Solid State Chem. 181 (2008) 685–692.
[15] J.C. Ruiz-Morales, J. Canales-Vázquez, J. Peña-Martínez, D. Marrero-López, J.T.S. Irvine, P. Núñez, J. Mater. Chem. 16 (2006) 540–542.
[16] J. Sacanell, A.G. Leyva, M.G. Bellino, D.G. Lamas, J. Power Sources 195 (2010) 1786–1792.
[17] R. Pinedo, I. Ruiz de Larramendi, D. Jimenez de Aberasturi, I. Gil de Muro, J.I. Ruiz de Larramendi, M.I. Arriortua, T. Rojo, J. Power Sources 196 (2011) 4174–4180.
[18] W. Sun, Z. Shi, S. Fang, L. Yan, Z. Zhu, W. Liu, Int. J. Hydrogen Energy 35 (2010) 7925–7929.
[19] Z. Qingjun, W. Fang, S. Yu, H. Tianmin, J. Power Sources 195 (2010) 2174–2181.
[20] J.H. Kim, Y.N. Kim, S.M. Cho, H. Wang, A. Manthiram, Electochim. Acta 55 (2010) 5312–5317.
[21] N. Ortiz-Vitoriano, I. Ruiz de Larramendi, J.I. Ruiz de Larramendi, M.I. Arriortua, T. Rojo, J. Power Sources 196 (2011) 4332–4336.
[22] N. Ortiz-Vitoriano, I. Ruiz de Larramendi, I. Gil de Muro, A. Larrañaga, J.I. Ruiz de Larramendi, T. Rojo, J. Mater. Chem. 21 (2011) 9682–9691.
[23] Z. Yang, Y. Huang, B. Dong, H. Li, Mater. Res. Bull. 41 (2006) 274–281.
[24] N. Ortiz-Vitoriano, I. Ruiz de Larramendi, I. Gil de Muro, J.I. Ruiz de Larramendi, T. Rojo, Mat. Res. Bull. 45 (2010) 1513–1519.
[25] J. Sacanell, M.G. Bellino, D.G. Lamas, A.G. Leyva, Physica B 398 (2007) 341–343.
[26] M.G. Bellino, J.G. Sacanell, D.G. Lamas, A.G. Leyva, N.E. Walsoe de Reca, J. Am. Chem. Soc. 129 (2007) 3066–3067.
[27] J. Rodríguez-Carvajal, Physica B 192 (1993) 55–69.
[28] H. Taimatsu, K. Wada, H. Kaneko, H. Yamamura, J. Am. Ceram. Soc. 75 (1992) 401–405.
[29] V. Gil, J. Tartaj, C. Moure, J. Eur. Ceram. Soc. 29 (2009) 1763–1770.
[30] Y.M. Yin, M.W. Xiong, N.T. Yang, Z. Tong, Y.Q. Guo, Z.F. Ma, E. Sun, J. Yamanis, B.Y. Jing, Int. J. Hydrogen Energy 36 (2011) 3989–3996.
[31] K. Park, C. Lee, J. Bae, Y. Yoo, Int. J. Hydrogen Energy 34 (2009) 6852–6860.
[32] P.K. Patro, T. Delahaye, E. Bouyer, Solid State Ionics 181 (2010) 1378–1386.
[33] N. Li, B. Wei, Z. Lü, X. Huang, W. Su, J. Alloys Compd. 509 (2011) 3651–3655.
[34] J.J. Roa, J.C. Ruiz-Morales, J. Canales-Vázquez, M. Morales, X.G. Capdevila, P. Núñez, M. Segarra, Fuel Cells 11 (2011) 124–130.
[35] B.D. White, O. Kesler, L. Rose, J. Power Sources 178 (2008) 334–343.
[36] T. Montini, M. Bevilacqua, E. Fonda, M.F. Casula, S. Lee, C. Tavagnacco, R.J. Gorte, P. Fornasiero, Chem. Mater. 21 (2009) 1768–1774.
[37] X. Zhou, P. Wang, L. Liu, K. Sun, Z. Gao, N. Zhang, J. Power Sources 191 (2009) 377–383.
[38] C. Sun, R. Hui, J. Roller, J. Solid State Electrochem. 14 (2010) 1125–1144.
[39] P. Hjalmarsson, M. Søgaard, A. Hagen, M. Mogensen, Solid State Ionics 179 (2008) 636–646.
[40] R. Barford, M. Mogensen, T. Klemensø, A. Hagen, Y.L. Liu, P.V. Hendriksen, J. Electrochem. Soc. 154 (2007) B371–B378.
[41] C. Bernuy-López, R. Knibbe, Z. He, X. Mao, A. Hauch, K.A. Nielsen, J. Power Sources 196 (2011) 4396–4403.
[42] X. Chen, S. Wang, Y.L. Yang, L. Smith, N.J. Wu, B.I. Kim, S.S. Perry, A.J. Jacobson, A. Ignatiev, Solid State Ionics 146 (2002) 405–413.
[43] N.T. Hart, N.P. Brandon, M.J. Day, J.E. Shemilt, J. Mater. Sci. 36 (2001) 1077–1085.
[44] B. Kenney, K. Karan, J. Electrochem. Soc. 153 (2006) A1172–A1180.
[45] S.B. Adler, Chem. Rev. 104 (2004) 4791–4843.
[46] H.X. Gu, Y. Zheng, R. Ran, Z.P. Shao, W.Q. Jin, N.P. Xu, J. Ahn, J. Power Sources 183 (2008) 471–478.
[47] T. Horita, K. Yamaji, N. Sakai, H. Yokokawa, A. Weber, E. Ivers-Tiffée, Electrochim. Acta 46 (2001) 1837–1845.
[48] S.B. Adler, Solid State Ionics 135 (2000) 603–612.
[49] Y. Fu, Int. J. Hydrogen Energy 36 (2011) 5574–5580.
[50] A. Dutta, J. Mukhopadhyay, R.N. Basu, J. Eur. Ceram. Soc. 29 (2009) 2003–2011.
[51] R. Pinedo, I. Ruiz de Larramendi, D. Jimenez de Aberasturi, I. Gil de Muro, A.T. Aguayo, J.I. Ruiz de Larramendi, T. Rojo, J. Mater. Chem. 21 (2011) 10273–10276.
[52] J. Wang, A. Manivannan, N. Wu, Thin Solid Films 517 (2008) 582–587.
[53] N. Zhang, J. Li, Z. He, K. Sun, Electrochem. Commun. 13 (2011) 570–573.
[54] M. Zhi, N. Mariani, R. Gemmen, K. Gerdes, N. Wu, Energy Environ. Sci. 4 (2011) 417–420.
[55] L. Li, P. Zhang, R. Liu, S.M. Guo, J. Power Sources 196 (2011) 1242–1247.
[56] B. Liu, X. Chen, Y. Dong, S.S. Mao, M. Cheng, Adv. Energy Mater. 1 (2011) 343–346.
[57] B. Wei, E.Z. Lu, X.Q. Huang, J.P. Miao, X.Q. Sha, X.S. Xin, W. Su, J. Eur. Ceram. Soc. 26 (2006) 2827–2832.